

Quantifying Wind Speed Effects on PV Array Thermal Behavior and Loads in an Agrivoltaic System: A Numerical Approach[#]

Ali Hesami^{1*}, Rebei Bel Fdhila^{1,2}, Mohammed Guezgouz¹, Pietro Elia Campana¹

1 Mälardalen University, Västerås, Sweden

2 Hitachi Energy Research, Forskargränd 7, 72178 Västerås, Sweden

(* Corresponding Author: ali.hesami@mdu.se)

ABSTRACT

This study presents a computational fluid dynamics analysis to quantify the influence of wind speed on the microclimate and aerodynamic performance of vertical bifacial photovoltaic arrays within an agrivoltaic system. The simulations are conducted using the experimental facility in Kärrobo Prästgård in Sweden (59.5545° N, 16.7625° E), composed of three rows of fixed, vertical bifacial photovoltaic modules. A series of numerical simulations were performed for four wind profiles with reference velocity ranging from 1 m/s to 15 m/s. The boundary conditions for ambient temperature, wind velocity profile (logarithmic inlet via user-defined function), and incident solar irradiance refer to June 23, 2022. The standard k-ε turbulence model was adopted to resolve turbulent atmospheric flow, while radiative heat transfer was captured using the discrete ordinates radiation model. Simulated panel surface temperatures were rigorously validated against published field measurements. The results demonstrate a strong dependence of aerodynamic forces on wind speed, with higher wind velocities significantly enhancing both convective heat transfer and mechanical loading on the PV structures. Specifically, the panel temperature decreases by 42% as the reference wind speed increases from 1 m/s to 15 m/s, while the wind load intensifies by a factor of 191. These findings underscore the critical influence of wind-induced effects on the thermo-structural performance of agrivoltaic systems and highlight the importance of integrated CFD-based assessments for their design and resilience optimization.

Keywords: Agrivoltaics, CFD, Microclimate Modeling, Renewable Energy

NOMENCLATURE

Abbreviations

APV	Agrivoltaic
CFD	Computational Fluid Dynamics
DO	Discrete Ordinates
FVM	Finite Volume Method
RANS	Raynolds-Averaged Navier-Stokes
RTE	Radiative Transfer Equation(s)
PV	Photovoltaic

Symbols

C_d	Drag coefficient
U_{ref}	Reference velocity
F_d	Drag force
ρ	Air density
μ	Dynamic viscosity
Re	Reynolds number
L	Characteristic length
Y^+	Normalized distance from wall
h	Convective heat transfer coefficient

1. INTRODUCTION

The rapid expansion of solar energy has increased competition between electricity generation and food production, as large-scale photovoltaic (PV) installations often require extensive land areas. Recent global analyses estimate that 13–16% of existing ground-mounted PV plants are located on land that previously served as cropland, highlighting the magnitude of this land-use conflict [1]. Agrivoltaic (APV) systems offer a promising solution by enabling the simultaneous use of land for both agriculture and PV electricity generation, thereby mitigating direct competition while maintaining productive farmland. Moreover, agrivoltaics has expanded rapidly, from 5 MWp in 2012 to 14 GWp worldwide by 2021,

demonstrating growing global interest in dual-use land strategies [2].

The investigation of microclimate has been studied through different methodologies including experimental measurements and numerical modeling [3]. Monitoring systems consist of different sensors being installed throughout the APV to collect temporal and spatial parameters such as temperature, humidity, soil moisture, and solar irradiance [4]. Then, they can be retrieved to crop models to evaluate crop growth performance. However, a generalized numerical model that can simulate the microclimate without conducting expensive field measurements has been always of great importance.

Computational Fluid Dynamics (CFD) is one of the high-fidelity numerical approaches to simulate multiphysics in a wide range of applications [5]. Previously, several CFD studies can be found in literature in both greenhouses [6] and APVs [3]. Although the greenhouse CFD studies are well investigated the coupling of crop activity and climate [6], APV needs more explorations to be well understood in the same aspect. In APV studies, Zainali et al. [7] developed a CFD model to simulate the microclimate within an APV experimental facility in Sweden consisting of three rows of vertical bifacial photovoltaic panels. They validated the model against field data for a 12-hour period starting from 5:00 to 17:00 on 23rd June 2022. The model predicted temperature distribution on panels and ground following with flow field patterns. In another study, Williams et. al. [8] developed CFD model to evaluate the cooling effect introduced by APV on conventional solar farms. They investigated panel height, surface albedo and evapotranspiration on panel surface temperature. In addition, the effect of panel height on panel and soil temperature is further investigated by Gong et. al. [9] using a thermal model based on CFD. The results showed that panel height has a regulatory effect on microclimate, leading to enhancement of heat exchange in the middle area. These recent studies identified the wind speed as a significant parameter that affects microclimate. Nevertheless, wind speed has not been sufficiently investigated on thermal modeling and load assessment of APV systems.

In this study, a CFD-based numerical model was developed to assess wind conditions in an experimental APV facility in Sweden. The model was validated against published module temperature measurements collected on 23rd June at 17:00 in a farmland area known as Kärro Prästgård located near Västerås [7]. Three representative time periods were selected to compare

the panel temperatures predicted by the CFD model with corresponding thermal camera observations. Subsequently, the validated model was employed to evaluate panel surface temperatures and aerodynamic forces under four distinct wind profile conditions.

2. METHODS

2.1 Problem definition

The APV facility investigated in this study consists of three rows of vertical bifacial solar panels, providing approximately 2500 m² of farmland for cultivation. Each array comprises 20 modules mounted in two vertically stacked rows. The geometric specifications of a single bifacial module are summarized in Table 1. As shown in Figure 1, for computational efficiency, each PV array was modeled as a single block to simplify the mesh generation process. Figure 1 also illustrates numerical domain and global coordinates used in this study.

The APV system operates as a coupled thermal–fluid domain, involving radiative, convective, and conductive heat transfer, combined with turbulent airflow. Additionally, mass transfer occurs between the crop layer and the atmosphere through evapotranspiration. However, in this study, evapotranspiration was neglected to simplify the model, as other heat transfer and aerodynamic mechanisms were considered to have a more dominant influence on the system’s behavior.

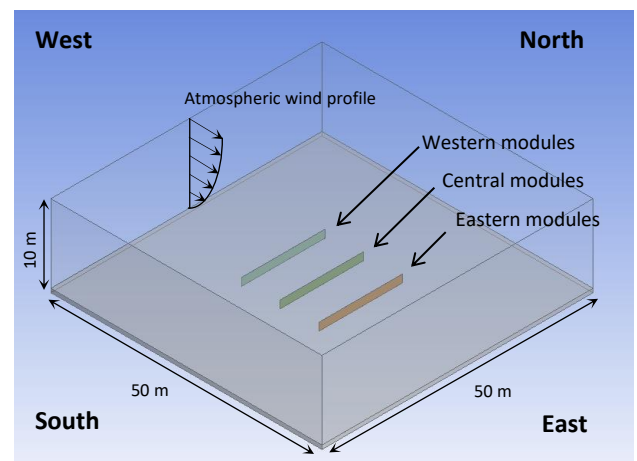


Figure 1: Numerical domain and APV layout.

2.2 Solver setting

The computational model numerically solves the governing conservation equations using the finite volume method on a discretized computational domain. Simulations were performed using the commercial code ANSYS Fluent v24 R1 [10, 11]. The Reynolds-Averaged Navier–Stokes (RANS) equations were solved in

conjunction with the standard $k-\epsilon$ turbulence model, applied at every control volume in the generated mesh. Radiative heat transfer was modeled using the Discrete Ordinates (DO) method, which was coupled with the Solar Load Model to compute site-specific solar heat fluxes based on the facility's global coordinates and the selected simulation dates.

2.3 Computational grid and boundary conditions

The numerical domain was discretized into a finite number of nodes, enabling the solution of the governing equations using the finite volume method (FVM). Structured quadrilateral elements were generated throughout the three-dimensional geometry, encompassing the soil layer, panel, and atmospheric region. Such structured grids generally achieve superior convergence characteristics compared to unstructured counterparts.

Appropriate boundary conditions were imposed on all numerical boundaries, as summarized in Table 2. The input parameters, namely solar irradiance, velocity, and temperature, were updated for each simulation time step. Specifically, irradiance parameters were incorporated into the solar load model, while the inlet boundary conditions were updated with the corresponding temperature values.

Table 1: Physical dimension of installed panels

Parameter	Single module (mm)	Array (mm)
Thickness	8	8
Length	2000	21500
Height	900	2000

Table 2: Boundary conditions

Boundary ID	Type
Inlet	Velocity inlet
Side walls	Wall (no-slip condition)
Panel and ground surfaces	Interface (mapped)
Outlet	Pressure outlet

Within atmospheric flows, the atmospheric boundary layer is assumed to follow a logarithmic profile given the terrain and reference velocity [12]. Thus, inlet wind profile is specified based on roughness height which is grassland with 10 cm height, and reference wind speed measured at weather station sensor unit located on 2 m height. Therefore, velocity profile is assigned at the inlet boundaries through User Defined Function

(UDF). This UDF consists of a logarithmic function, measuring the velocity component for every node at inlet boundaries based on its distance from ground level.

Four reference wind speeds are considered including 1, 5, 10, 15 m/s that create four wind profiles to study the wind speed effect. It is worth noting that roughness height was kept constant as the crop height is not on the scope of present study.

3. RESULTS

3.1 Validation study

To ensure the reliability of the developed CFD model, validation against experimental and/or theoretical data is essential. Published field measurements available in the literature were therefore used as reference data for comparing the numerical predictions with observed conditions. Accordingly, key input parameters, including solar irradiance, wind speed, and ambient temperature, were specified based on measurements obtained from the APV test facility. This approach ensures that the boundary conditions and environmental inputs used in the simulations accurately reflect the real operating conditions of the experimental site, thereby strengthening the credibility of the model's predictive performance.

Thermal camera measurements of panel temperature reported by Zainali et al. [7] were used in this study, and the results are compared to validate the present CFD simulation reported in the Figure 2. A maximum deviation of 5 °C is observed at 14:00, corresponding to 16% of the experimental value. This discrepancy arises because the thermal camera data was obtained at a single, unspecified point, while the CFD results report the average temperature over the entire array.

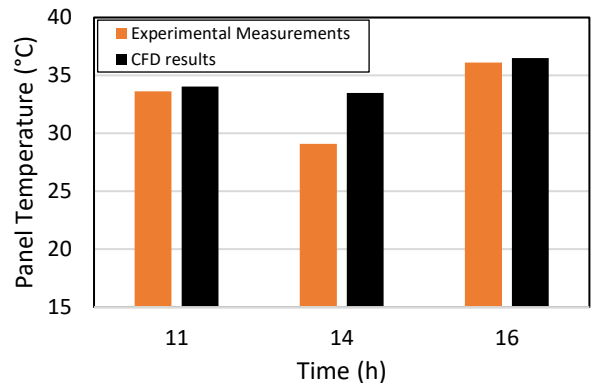


Figure 2: Validation results for three representative hours.

3.2 Temperature distribution

Average panel temperature on three arrays is reported in Figure 3 corresponding to $U_{ref}=1\text{ m/s}$, $U_{ref}=10\text{ m/s}$, and $U_{ref}=15\text{ m/s}$. It decreases significantly as the reference velocity increases. Although it has a descending trend for all arrays, the largest temperature drop was observed on $U_{ref}=5\text{ m/s}$. In Figure 4, temperature contours are also plotted on panels and ground surfaces for three specific wind profiles. The results indicate that the ground-surface temperature distribution decreases with increasing wind speed, mirroring the reduction observed in module temperature. Furthermore, regions of lower temperature appear downstream of the PV arrays and within shaded zones. These patterns correspond to enhanced convective heat transfer in the wake of the panels and reduced solar heat flux in shaded areas, respectively.

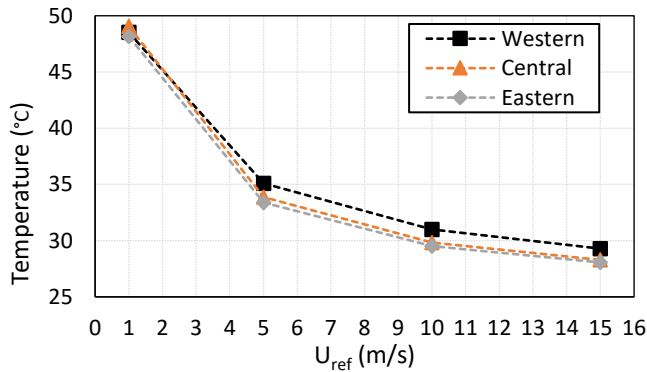


Figure 3: Average temperature on arrays versus wind flows.

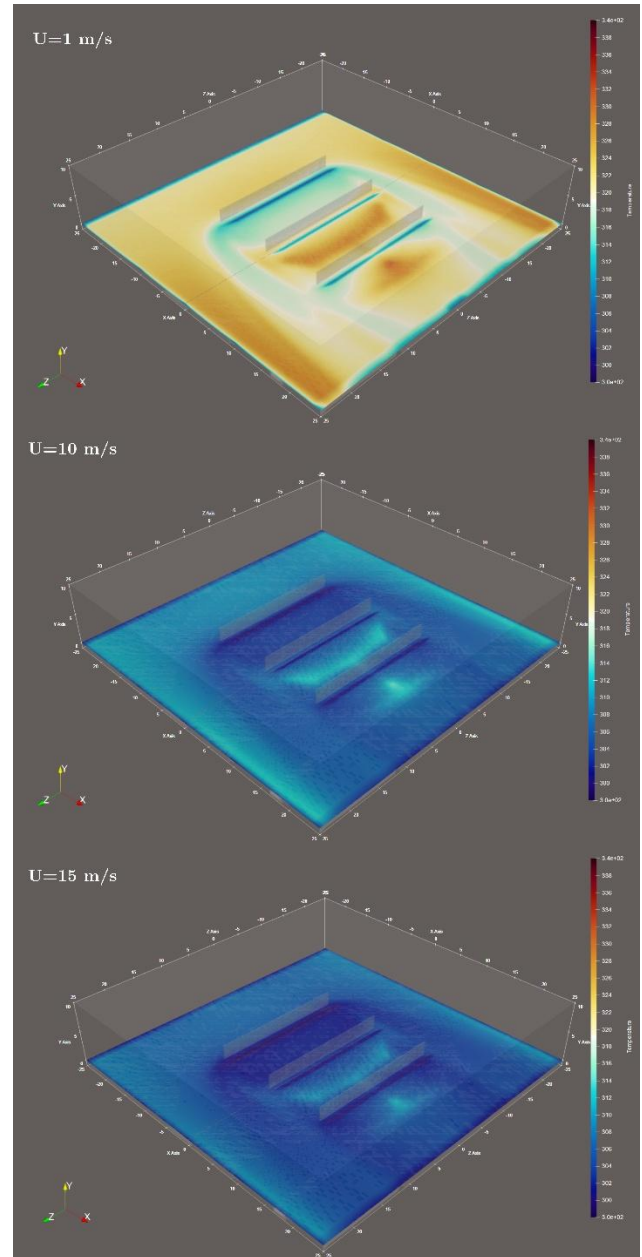


Figure 4: Temperature distribution on panel and ground surfaces.

3.3 Wind load assessment

Wind flow exerts drag force on PV arrays within the APV depending on flow velocity and geometrical shape. However, wind speed is the only parameter that is investigated in the present study. In Figure 5, total drag forces are plotted for different wind profiles on three arrays in the APV. The results show all arrays experience the same increasing trend with accelerating wind speed. Additionally, western, eastern, and central arrays respectively have the highest value, because the prevailing wind direction was assumed to pass from west to east. This results in a relatively large wake region

downstream of western array, leading to reduce aerodynamic loads on the other two. This is further studied in the discussion.

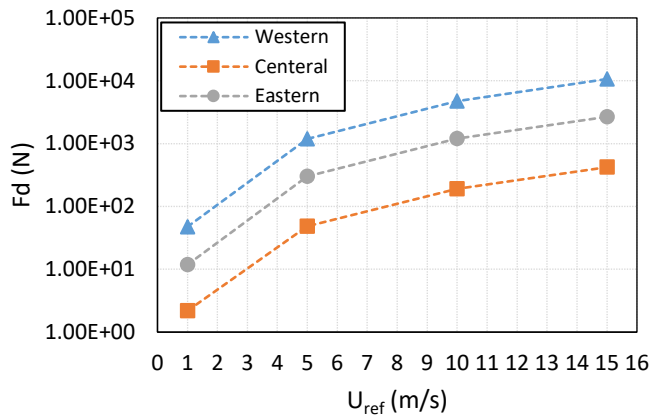


Figure 5: Applied force on arrays versus wind flows.

4. DISCUSSION

Figure 3 reports the average panel surface temperature for the western, central, and eastern arrays as a function of reference wind speed. The data show a clear monotonic cooling with increasing wind speed, with the largest incremental drop occurring between 1 and 5 m/s. This non-linear behavior is physically consistent with an external forced-convection balance on a sunlit vertical plate: the convective heat transfer coefficient (h) scales roughly as $h \sim U_{ref}^n$ with $n \approx 0.6 - 0.8$ for cross-flow over bluff plates at these Reynolds numbers ($Re = \rho UL/\mu$) [13]. As the reference wind speed U_{ref} increases, the air density (ρ), characteristic length (L), and dynamic viscosity (μ) remain constant; consequently, the external forced-convection boundary layer becomes thinner. This enhanced convective transport increases the heat transfer coefficient, causing the surface temperature to asymptotically approach the ambient temperature as convective heat removal increasingly dominates the overall energy balance. The strong initial cooling from 1 m/s to 5 m/s reflects a transition from mixed to forced convection; further increases to 10–15 m/s yield diminishing returns because h grows sublinearly while the radiative terms are relatively insensitive to wind speed.

Figure 4 shows a 3-D domain with three vertical, solar arrays and a temperature field (about 300–340 K) rendered on a near-ground slice and on the panel faces for three inflow speeds $U_{ref} = 1, 10, \text{ and } 15 \text{ m/s}$. At $U_{ref} = 1 \text{ m/s}$ the domain is generally warmer, with broad high-temperature patches and clearly visible cool streaks just

downstream of each panel; the wakes are long and thermally distinct, and the ground shading by the vertical plates is imprinted as cooler bands. When the speed increases to 10 and 15 m/s the field becomes colder and more uniform, and the wakes shorten and blur because turbulent mixing and entrainment are stronger. A localized hot patch persists near the right side of the central array (Figure 4) in all three cases, due to weakly ventilated area created by upstream arrays.

For system implications, the cooler and more uniform fields at 10–15 m/s imply lower panel temperatures and a small efficiency gain for PV modules (typical temperature coefficient about -0.3 to -0.5% per kelvin [14]), balanced by higher mechanical loads. The clear wake signatures at low wind speed show that panel spacing controls interference; tight gaps can merge wakes into a broad cool trench, whereas at higher wind speed the layout shifts to end effects, consistent with the persistent hot spot.

Figure 4 presents total drag forces on each array for the four wind profiles. The trend is near-quadratic in U_{ref} . The ordering—western > eastern > central—indicates (i) the leading western row bears the full undisturbed dynamic pressure, (ii) the middle row sits in the deepest wake and thus sees the smallest loads, and (iii) the eastern row benefits from partial wake recovery and possible channeling between rows that re-accelerates the flow locally. All curves rise steeply with wind, consistent with the quadratic relation of drag force ($F_d = 0.5 \rho C_d A U_{ref}^2$), but the three rows do not carry the same load. The Western (windward) row is highest at every speed, the Eastern row is intermediate, and the Central row is the lowest, which indicates shielding of interior panels by upstream wakes.

Practically, the data argue for edge strengthening and possibly increased spacing or staggering at the windward side to reduce exposure, for array-level gust factors rather than single-panel coefficients in design, and for fatigue checks, because the strong nonlinearity means small increases in site wind or gustiness can produce order-of-magnitude increases in structural load.

5. CONCLUSIONS

This work addressed how wind speed reshapes the thermal modelling of microclimate and the mechanical load on a three-row vertical PV array. Using a CFD model coupled with solar radiation and temperature data validated against thermal imagery, we quantified the trade-off between cooling and load as the reference inlet

wind increased from 1 to 15 m/s. The results indicated that:

- 1) The array's average panel temperature decreases markedly with wind, dropping by about 42% from 1 to 15 m/s, with the largest incremental reduction between 1 and 5 m/s
- 2) Total drag grows near-quadratically with wind and increases by a factor of ~191 across the same range; row wise loads order Western > Eastern > Central because the windward row bears undisturbed flow while middle rows are wake-shielded.
- 3) Low winds yield radiation-dominated, patchy warm fields with long wakes and clear ground-shade bands; higher winds homogenize temperatures and shorten wakes through stronger mixing, with a localized hotspot tied to geometry/boundary conditions rather than convection alone.
- 4) Cooling benefits suggest modest PV efficiency gains at higher winds, but the sharply rising loads necessitate edge reinforcement, spacing/staggering to manage interference, and array-level gust factors. The results motivate integrated CFD-based thermo-structural assessments for resilient APV design.

[7] Zainali S, et al. Computational fluid dynamics modelling of microclimate for a vertical agrivoltaic system. *Energy Nexus* 2023;9:100173.

[8] Williams HJ, Hashad K, Wang H, Zhang KM. The potential for agrivoltaics to enhance solar farm cooling. *Applied Energy* 2023;332:120478.

[9] Gong W, et al. Regulatory effect of agriphotovoltaic systems with different panel heights on the thermal environment. *Scientific Reports* 2025;15(1):11196.

[10] ANSYS Inc. ANSYS Fluent theory guide. ANSYS Inc.; 2011.

[11] ANSYS Inc. ANSYS Fluent user's guide. ANSYS Inc.; 2011.

[12] Blocken B, Stathopoulos T, Carmeliet J. CFD simulation of the atmospheric boundary layer: wall function problems. *Atmospheric Environment* 2007;41(2):238–252.

[13] Incropera FP, DeWitt DP, Bergman TL, Lavine AS. *Fundamentals of heat and mass transfer*. Wiley; 1996.

[14] Niclas (2016). Measuring the Temperature Coefficient of a PV Module. Retrieved from <https://sinovoltaics.com/solar-basics/measuring-the-temperature-coefficients-of-a-pv-module/>.

REFERENCE

[1] Curioni M, Galli N, Manzolini G, Rulli MC. Global land-water competition and synergy between solar energy and agriculture. *Earth's Future* 2025;13(2):e2024EF005291.

[2] Mahim TM, Rahman MM, Huda AN. Review of the challenges and prospects in agrivoltaics. *Advanced Energy and Sustainability Research* 2025;:2500227.

[3] Zainali S, et al. Modelling, simulation, and optimisation of agrivoltaic systems: a comprehensive review. *Applied Energy* 2025;386:125558.

[4] Rebaudo F, et al. A low-cost IoT network to monitor microclimate variables in ecosystems. *Methods in Ecology and Evolution* 2023;14(4):1025–1034.

[5] Versteeg HK. *An introduction to computational fluid dynamics: the finite volume method*. 2nd ed. Pearson Education India; 2007.

[6] Fatnassi H, Bournet PE, Boulard T, Roy JC, Molina-Aiz FD, Zaaboul R. Use of computational fluid dynamic tools to model the coupling of plant canopy activity and climate in greenhouses and closed plant growth systems: a review. *Biosystems Engineering* 2023;230:388–408.